

# Efficient Mapping of On-Demand Drive Load Profiles on Inverter Stress

Zlatko Bosnjic<sup>1</sup>, Klaus Krischan<sup>1</sup>, Franz Königseder<sup>2</sup>, Alexander Loibl<sup>2</sup>, Michael Hartmann<sup>1</sup>

<sup>1</sup> Electric Drives and Machines Institute, Graz University of Technology, Graz, Austria

<sup>2</sup> Magna, Austria

Corresponding author: Zlatko Bosnjic, zlatko.bosnjic@tugraz.at

Speaker: Zlatko Bosnjic, zlatko.bosnjic@tugraz.at

## Abstract

Mechanical and thermal stresses of EV drive system components strongly depend on how the drive is operated during its lifetime. In On-Demand drives, expected operation is difficult to quantify as it depends on vehicle design, powertrain design and torque distribution strategy. This paper proposes two methods for generating representative On-Demand drive Load Profiles based on vehicle speed profiles. Additionally, a compact drive system model for efficient simulation of traction inverter thermal stress is derived and explained in detail. The inverter thermal stress is simulated for a measured On-Demand speed/torque profile and is compared to simulation results based on the two proposed methods. The results show good match between measured and generated drive loading profiles.

## 1 Introduction

Interest in battery electric vehicles (BEVs) has been growing rapidly in recent years [1] as the need for sustainable transportation is becoming more obvious [2]. Benefits of BEVs are quite clear and have been analyzed and discussed in-depth ([1], [3] and [4]). BEVs usually employ only one traction motor (single-motor EVs), however, for applications and driving scenarios where additional performance, stability and reliability is desired, electric vehicles with more than one traction motor (multi-motor EVs) are preferred ([2] and [5]). Dual-motor EVs, with one traction motor on each vehicle axle are the largest subgroup of multi-motor EVs. In Fig. 1, a schematic depiction of such EV powertrains is shown. Depending on vehicle requirements and system design, the two drive systems in a dual-motor EV can range from being almost equal and working in parallel to substantially different in design where one drive is only used for acceleration and stability. Based on benchmark reports of commercial EVs, the latter is a more common solution. The two drive systems found in dual-motor EVs are designated as:

- Main (primary) drive system, and
- On-Demand (secondary) drive system.

As the On-Demand drive may supply torque only when required for acceleration or stability, the mission profile of such a drive differs from the main drive (and from the drive system in a single-motor EV). Due to this, the lifetime requirements imposed on components of the On-Demand drive system also differ from that of a single-motor EV drive system. The discrepancy of main drive usage and On-Demand drive usage has also been verified by measurements from real-world driving scenarios of a dual-motor EV and is presented in Fig. 2.

Although dual-motor EVs have been in the scope of research for some time, there appears to be a lack of published data regarding the differences in usage and lifetime requirements of the two drive systems. The main drive system in a dual-motor EV is similar in design and usage to a single-motor EV drive system. It is therefore not considered in this work as there is a great deal of publications covering standard single-motor EVs ([6] and [7]). Another topic addressed in this paper is accurate prediction of semiconductor junction temperature profiles. Usually, accurate simulation of junction temperatures relies on FEM and is computationally intensive. Therefore it is not used for system level optimization in EV powertrain design. A computationally efficient electro-thermal model, including

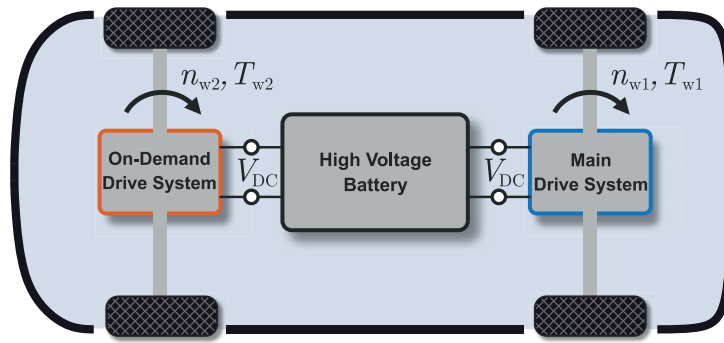


**Fig. 1:** Schematic of dual-motor EV power-train consisting of main drive system and On-Demand drive system.

thermal coupling between chips, is proposed in this paper as a substitute for FEM.

This paper provides an outline for a more optimal inverter stage design of the On-Demand drive system by addressing the influence of vehicle speed profiles on On-Demand drive inverter thermal stress. The approach presented here can be subdivided into a two step process:

1. Accurate mapping of vehicle speed profiles  $v_v(t)$  to On-Demand drive speed  $n_2(t)$  and On-Demand drive torque  $T_2(t)$  by means of a novel torque mapping method, and
2. Efficient simulation of inverter thermal stress based on drive speed  $n_2(t)$  and drive torque  $T_2(t)$ .

The rest of the paper is structured as follows: **Section 2** provides an in-depth analysis of the derivation of On-Demand drive loading in dual-motor EVs. In **Section 3** the thermal stresses of the On-Demand drive inverter are simulated based on results from **Section 2**. The results of thermal stress simulation for different torque mapping approaches are presented and discussed in **Section 4**. Finally, in **Section 5**, a conclusion and outlook for further work is given.

## 2 On-Demand Drive Usage

The usage of the On-Demand drive system in dual-motor EVs is not easily defined, especially during the design phase. The usage criteria of the On-Demand drive is a result of a superimposed torque distribution control strategy which determines how the required torque is generated across the two drives in a dual-motor EV. This control strategy is often based on overall system loss minimization ([8], [9]) and requires detailed knowledge on both

the vehicle model and the drive system design(s). Here, the usage of the On-Demand drive is derived from simplified criteria and measurement data without prior information on torque distribution. In Fig. 1, a schematic of a dual-motor EV powertrain is depicted.

For a representative speed/torque profile of the On-Demand drive ( $T_2(t), n_2(t)$ ), the following should be known:

- Representative vehicle speed profile  $v_v(t)$  (e.g. WLTC speed profile)
- Longitudinal vehicle model (vehicle mass -  $m_v$ , drag area -  $C_dA$ , rolling resistance -  $\mu_r$ , etc.)
- Primary drive specification
- Secondary drive specification
- Torque distribution strategy

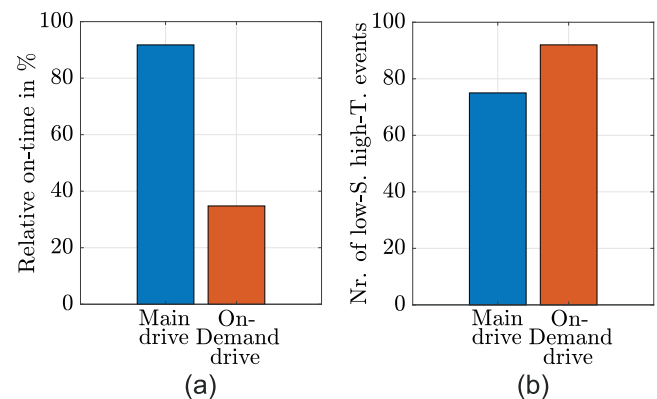


**Fig. 2:** Primary drive and On-Demand drive usage obtained from measurement data. (a) Relative on-time and (b) Number of low speed - high torque events.

A drive system design based only on standard peak drive torque  $T_{pk}$  and peak drive power  $P_{pk}$  requirements might lead to oversized drive components.

It is therefore necessary to also address the expected drive system usage as one of the design requirements.

In Fig. 2, a comparison of main drive and On-Demand drive usage is shown. The usage comparison has been extracted from data collected over 10 hours of measurements across different driving scenarios and it can be assumed that the driving scenarios are representative of expected usage for the particular EV. Measurement data indicates that the total on-time of the On-Demand drive is much lower compared to the main drive (by a factor of 2.5 - Fig. 2 (a)). However, the number of "low speed - high torque" events is higher for the On-Demand drive (Fig. 2 (b)). Each operating point of the traction machine for which the machine produces above 80 % of it's rated peak torque at an electrical frequency of 5 Hz or less is considered as "low speed - high torque". These events usually have the largest impact on lifetime degradation [6]. In order to address the topic of On-Demand drive usage and subsequently lifetime degradation of the drive components, representative drive loading profiles should firstly be established. This paper proposes two approaches for generation of representative drive loading profiles:

1. Speed/torque derivation based on vehicle model and simplified On-Demand usage criteria - (**Approach A** in Fig. 3), and
2. Speed/torque derivation based on vehicle model and torque mapping - (**Approach B** in Fig. 3).

For both approaches, a simplified longitudinal vehicle model is assumed. Model dynamics are defined by

$$m_v \dot{v}_v(t) = \frac{T_w(t)}{r_w} - \sum F_i(t) \quad (1)$$

where  $m_v$  is the vehicle mass,  $r_w$  is the wheel radius,  $v_v(t)$  is the vehicle speed,  $T_w(t)$  is the required wheel torque and  $\sum F_i$  is the sum of all forces acting on the vehicle in the longitudinal direction. External forces acting on the vehicle can be divided into the aerodynamic drag force, frictional force and gravitational force

$$\sum F_i(t) = \frac{\rho_{\text{air}}}{2} C_d A v_v^2(t) + m_v g (\sin \alpha + \mu_r \cos \alpha). \quad (2)$$

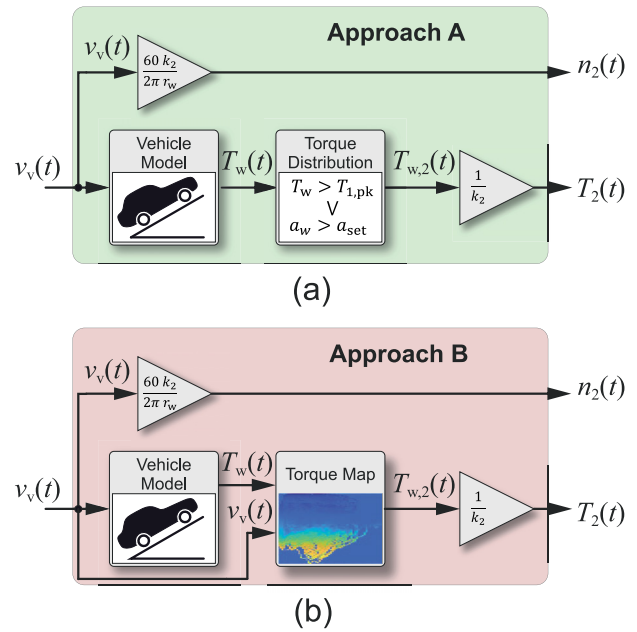


**Fig. 3:** Generation of On-Demand drive torque profiles based on (a) - vehicle model and control strategy - **Approach A** and (b) vehicle model and On-Demand torque map - **Approach B**.

In (2),  $\rho_{\text{air}}$  designates the density of air and  $\alpha = \alpha(t)$  designates the inclination (slope) profile of the terrain. The required wheel torque is generated by the main drive system and the On-Demand drive system

$$T_w(t) = k_1 T_1(t) + k_2 T_2(t) \quad (3)$$

where  $k_1$  and  $k_2$  are the gearbox ratios of the main drive and On-Demand drive, respectively. The vehicle dynamics given in (1) provide a value for the required wheel torque, however the distribution of main drive torque  $T_1$  and On-Demand drive torque  $T_2$  is not specified. Employing either **Approach A** or **Approach B**, as presented in Fig. 3, it is possible to obtain this torque distribution for a dual-motor EV ( $T_1(t)$  and  $T_2(t)$  in (3)).

As an example of drive control strategy for **Approach A**, the On-Demand drive produces torque when the required wheel torque is higher than the peak torque that the main drive can produce

$$T_w(t) > k_1 T_{1,\text{pk}}. \quad (4)$$

As another example, the On-Demand drive is used when the required wheel torque is higher than some defined torque set-point  $T_{\text{set}}$

$$T_w(t) > T_{\text{set}}. \quad (5)$$

The mentioned On-Demand drive usage criteria are simplified and are usually not an accurate representation of real-world drive usage. Due to this, a torque mapping approach is presented here which aims to provide better accuracy in estimating secondary drive torque. The derivation of the torque map used in **Approach B**, is shown in Fig. 4.

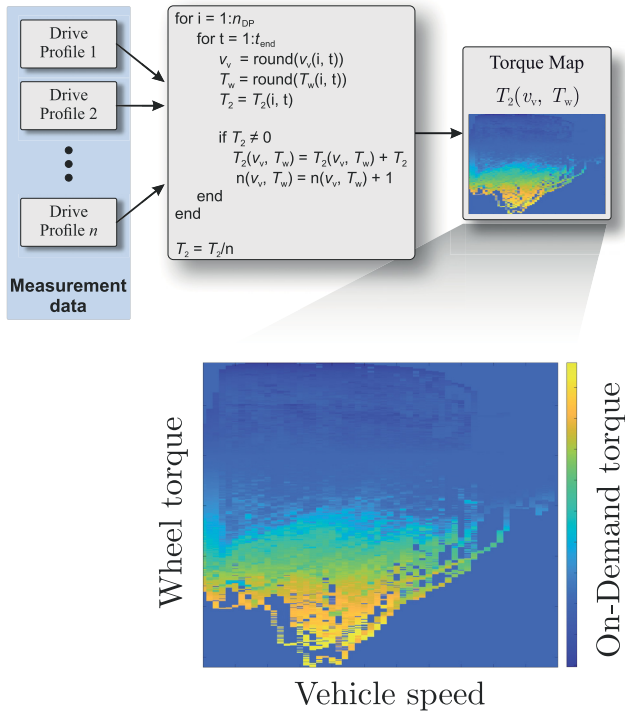


**Fig. 4:** Generation of On-Demand drive torque profiles based on vehicle model and vehicle measurement data.

This second approach is based on mapping of vehicle speed and vehicle wheel torque to On-Demand drive torque. The mapping has been extracted from vehicle measurement data as shown in Fig. 4 and is based on statistical correlation of the On-Demand drive torque to the vehicle speed and vehicle wheel torque. For each combination of vehicle speed  $v_v$  and vehicle wheel torque  $T_w$ , the expected value of the On-Demand torque has been calculated by

$$T_2(v_v, T_w) = \frac{\sum T_{2,\text{meas}}(v_{v,\text{meas}} = v_v, T_{w,\text{meas}} = T_w)}{N}. \quad (6)$$

In (6), the On-Demand drive torque map  $T_2(v_v, T_w)$  is calculated from measurement data  $T_{2,\text{meas}}$ ,  $v_{v,\text{meas}}$  and  $T_{w,\text{meas}}$ . Measurement data was binned into bins of width 1 m/s and 1 N m respectively. Although this approach inherently introduces "smoothing" into the generated torque profiles, it can serve as

a tool for accurate estimation of On-Demand drive torque. The proposed approach encodes relevant torque distribution data into a single 3D map without the need for *a priori* knowledge of the torque distribution control strategy. Therefore, it is possible to estimate the expected loading of the On-Demand drive without knowing the exact control strategy in a dual-motor EV. This 3D map can ultimately be used as a look-up table for generation of On-Demand drive torque profiles with arbitrary vehicle speed as input.

In Fig. 5, the derived On-Demand torque profiles for **Approach A** and **Approach B** are shown along with measured On-Demand torque for reference. A vehicle speed profile has been isolated from the measurement results in order to compare the validity of the approaches based on torque profile generation from the mentioned approaches. As can be seen, the generated torque profile from **Approach A** does not show good matching to the measured torque as the torque distribution strategy is not known and is only approximated by simple usage criteria. A better match might be achieved if the cut-in criteria is better approximated. **Approach B** shows much better matching with measured results.

For comparison, the first approach offers a lot more flexibility, where arbitrary torque profiles can be generated from vehicle speed profiles and vehicle parameters. This approach allows for freedom of choice where it is possible to iterate through different vehicle segments (e.g. compact vehicle to SUV) and different On-Demand drive usage strategies (e.g. secondary drive activated or continuously in operation in parallel with the main drive) by varying vehicle parameters and drive usage criteria as shown in (4) and (5). On the other hand, the torque mapping approach limits the flexibility in vehicle choice. As the torque map is derived from measurements in a single vehicle, the mapping is only representative of this vehicle.

### 3 Drive System Model

In the previous section, two methods for deriving On-Demand drive torque profiles from arbitrary vehicle speed profiles have been presented. The lifetime requirements of drive system components are highly dependent on these profiles as the mechanical and thermal stresses are a direct consequence of drive loading ([10] and [11]). In order to accurately predict thermal stress within a power module,

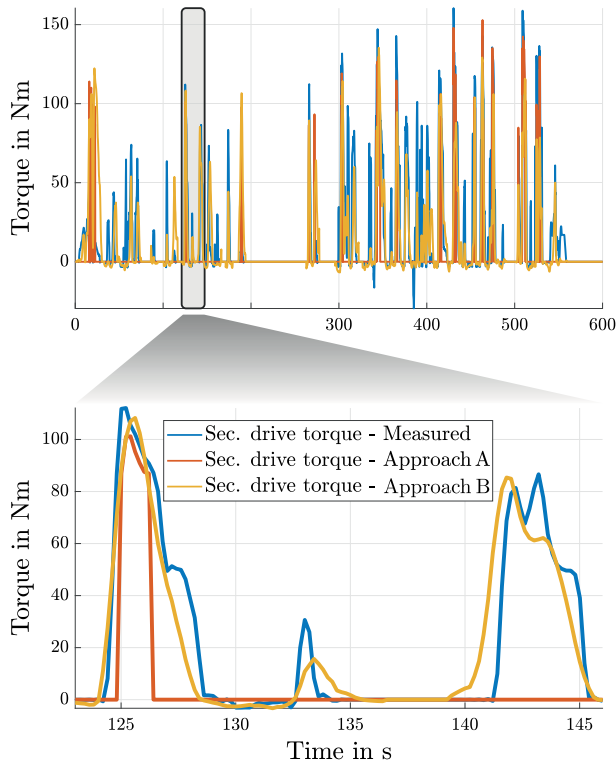


**Fig. 5:** Comparison of measured On-Demand drive torque with torque derived from cut-in criteria (**Approach A**) and torque derived from torque mapping (**Approach B**).

the expected junction temperature profiles need to be established. This section focuses on efficient simulation of On-Demand drive inverter temperatures for estimation of power module thermal stress. Compared to Finite Element Method simulation models, which are commonly employed for junction temperature estimation, the electro-thermal model presented here is much less computationally intensive, as it is based on a 1D Foster thermal network representation of the thermal system. In the first step, the speed/torque profile of the traction machine needs to be converted into machine voltages and currents. Next, the voltages and currents are to be transferred into power losses within the module and finally into junction temperature profiles of the semiconductors as shown in the block diagram in Fig. 6.

### 3.1 Traction Machine Model and Speed Control

For the traction machine of the On-Demand drive, a four-pole ( $p = 2$ ) Induction Machine (IM) is assumed. IM voltages  $u_m(t)$  and currents  $i_m(t)$  are obtained from equivalent circuit model impedance and the machine torque equation

$$\underline{Z} = R_1 + j \omega_{el} L_1 + j \omega_{el} L_m \parallel \left( \frac{R'_2}{s} + j \omega_{el} L'_2 \right) \quad (7)$$

$$T_{el} = \frac{3p}{\omega_{el}} \frac{R'_2 s U_m^2}{R_2^2 + (s \omega_{el} L'_2)^2} \quad (8)$$

where  $R_1$ ,  $L_1$ ,  $R'_2$ ,  $L'_2$  and  $L_m$  are equivalent circuit parameters of the induction machine,  $p$  is the number of pole-pairs,  $s = \frac{\omega_{el} - p \omega_{mech}}{\omega_{el}}$  is the slip and  $U_m$  is the magnetizing voltage. The model given in (7) and (8) does not uniquely define the voltage and current wave-forms of the IM for a given mechanical operating point (speed and torque). Therefore, an additional equation is required. The magnitude of the IM voltage as a function of rotational speed is defined as

$$\hat{U}_m = n_2 \frac{\hat{U}_{m,max}}{n_{2,max}}. \quad (9)$$

This is a simplification of speed control of induction machines in which the magnitude of the applied voltage at the stator is proportional to the rotational speed of the machine.

The set of equations (7) - (9) define the electrical operating point of the Induction Machine ( $\hat{U}_m$ ,  $\hat{I}_m$ ,  $\omega_{el}$  and  $\phi$ ) assuming known mechanical operating point ( $n_2$ ,  $T_2$ ). Machine voltages and currents are assumed to be sinusoidal

$$\begin{aligned} u_m(t) &= \hat{U}_m \cos(\omega_{el} t) \\ i_m(t) &= \hat{I}_m \cos(\omega_{el} t - \phi). \end{aligned} \quad (10)$$

### 3.2 Inverter electro-thermal model

With known motor voltages and motor currents, the current stress of inverter power semiconductors can be calculated. Finally, a detailed electro-thermal model of the inverter is implemented for junction temperature simulation. The electro-thermal model is based on a state-space representation of the module junction temperatures. The model is derived from the integral representation of the Foster thermal network [12]

$$T_j(t) - T_C = \int_0^t P(\tau) \dot{Z}_{th}(t - \tau) d\tau. \quad (11)$$

and can be extended to include thermal coupling effects of adjacent chips ( $i$ -th chip) within a power module, as well as Foster thermal networks of higher order ( $I_m$ ). The extended model is defined as

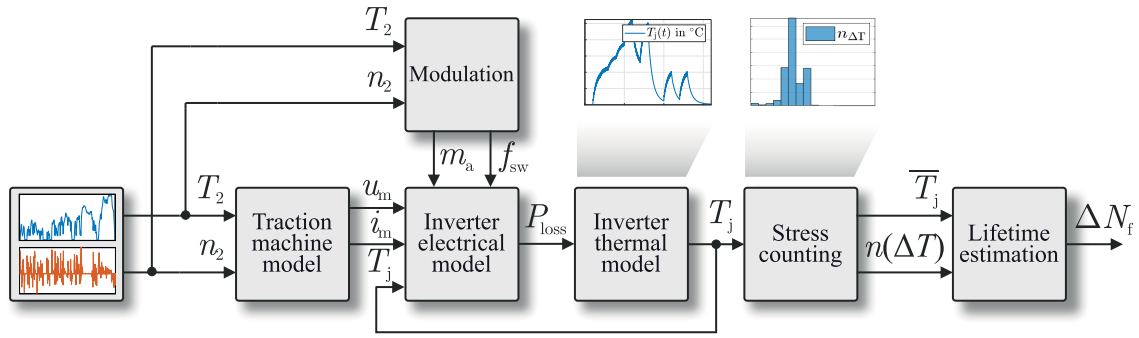


**Fig. 6:** Schematic overview of On-Demand drive system model used for junction temperature simulation.

$$T_j(t) - T_c = \sum_{i=1}^n \sum_{l=1}^{l_m} \frac{R_l}{\tau_l} \int_0^t P_i(\tau) e^{-(t-\tau)/\tau_l} d\tau \quad (12)$$

where  $T_j(t)$  is the junction temperature of the semiconductor,  $T_c$  is the coolant temperature,  $R_l$  is the thermal resistance of the  $l$ -th component in the Foster network of size  $l_m$  and  $P_i(t)$  is the generated power loss within the  $i$ -th switch.

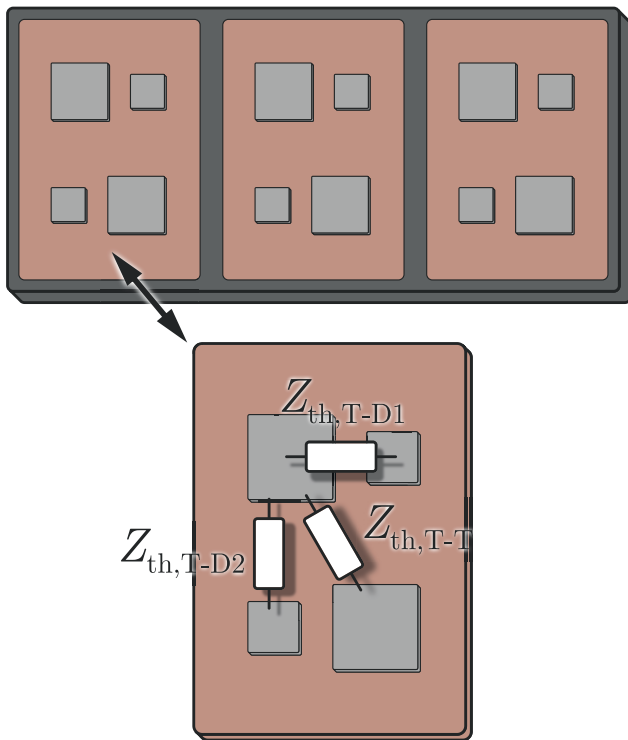


**Fig. 7:** Schematic of traction inverter power module with indicated thermal impedances.

In Fig. 7, a schematic representation of a six-switch power module is shown with indicated thermal coupling impedances ( $Z_{th,T-D1}$ ,  $Z_{th,T-T}$  and  $Z_{th,T-D2}$ ). For simulation, the thermal coupling impedances are modeled with a second order

Foster network, while the junction-coolant thermal impedance  $Z_{th,T-C}$  is represented with a fourth order Foster network

$$Z_{th,T-D1}(t) = \sum_{l=1}^2 R_{l,T-D1} (1 - e^{-t/\tau_{l,T-D1}}) \quad (13)$$

$$Z_{th,T-C}(t) = \sum_{l=1}^4 R_{l,T-C} (1 - e^{-t/\tau_{l,T-C}}).$$

The parameters of the Foster networks, as well as network order was determined from transient thermal measurements. Measurements show that there is minimal thermal coupling between adjacent bridge-legs within the power module and therefore only a single bridge-leg is considered although the model in (12) can be extended to include an arbitrary number thermal coupling impedances. Based on results presented in [13], it is possible to transform the integral representation of the coupled Foster network thermal model into a state-space representation

$$\frac{d\Delta\mathbf{T}_i(t)}{dt} = \mathbf{A}_i \Delta\mathbf{T}_i(t) + \mathbf{B}_i \mathbf{P}(t) \quad (14)$$

$$T_j(t) = \mathbf{C}_i \Delta\mathbf{T}_i(t) + T_c$$

Matrices  $\mathbf{A}_i$  and  $\mathbf{B}_i$  are derived from the integral representation of Foster thermal networks

$$\mathbf{A}_i = \begin{bmatrix} \mathbf{A}_{n1} & 0 \\ 0 & \mathbf{A}_{n2} \end{bmatrix}, \quad (15)$$

$$\mathbf{B}_i = \begin{bmatrix} \mathbf{B}_{n1} & 0 \\ 0 & \mathbf{B}_{n2} \end{bmatrix} \quad (16)$$

where

$$\mathbf{A}_{n1} = \begin{bmatrix} \frac{-1}{\tau_{1,T-C}} & 0 & 0 & 0 \\ 0 & \frac{-1}{\tau_{2,T-C}} & 0 & 0 \\ 0 & 0 & \frac{-1}{\tau_{3,T-C}} & 0 \\ 0 & 0 & 0 & \frac{-1}{\tau_{4,T-C}} \end{bmatrix}, \quad (17)$$

$$\mathbf{A}_{n2} = \begin{bmatrix} \frac{-1}{\tau_{1,T-D1}} & 0 \\ 0 & \frac{-1}{\tau_{2,T-D1}} \end{bmatrix} \quad (18)$$

and

$$\mathbf{B}_{n1} = \begin{bmatrix} \frac{R_{1,T-C}}{\tau_{1,T-C}} \\ \frac{R_{2,T-C}}{\tau_{2,T-C}} \\ \frac{R_{3,T-C}}{\tau_{3,T-C}} \\ \frac{R_{4,T-C}}{\tau_{4,T-C}} \end{bmatrix}, \mathbf{B}_{n2} = \begin{bmatrix} \frac{R_{1,T-D1}}{\tau_{1,T-D1}} \\ \frac{R_{2,T-D1}}{\tau_{2,T-D1}} \end{bmatrix}. \quad (19)$$

In (15) - (19) system matrices of a simplified state-space model with thermal coupling between the active switch and its freewheeling diode are shown. This simplified model is outlined here for clarity as the order of the full state-space system is  $\left(\sum_{i=1}^{N_i} N_k(i) \times \sum_{i=1}^{N_i} N_k(i)\right)$  where  $N_k$  is the number of Foster network elements and  $N_i$  is the number of considered thermal couplings. For the case of the model which includes only one thermal coupling (switch to its diode) for the matrices given in (15) - (19), the order of the system is  $6 \times 6$ .

The state-space representation of a power module thermal network is easy to implement for simulation and the time-discrete model offers fastest run-time (Fig. 8). The run-time of three model representations has been evaluated for a simplified thermal system - half-bridge with full thermal coupling.

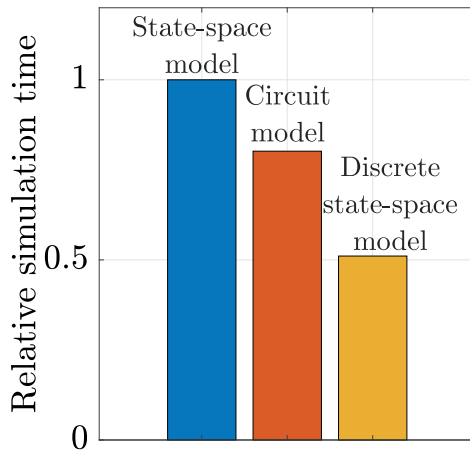


**Fig. 8:** Comparison of relative run-time for different implementations of the thermal model.

In total, 10 000 electrical periods have been simulated in order to reduce the influence of model initialization on simulation run-time. The model representations have also been compared with different simulation software. Additionally, the accuracy of the different representations has been evaluated against each other and shows a good match.

## 4 Results and discussion

The simulated drive system is based on a six-pack IGBT power module with a nominal DC-Link voltage of 400 V coupled to a four-pole induction machine (IM). The specification of the drive system is given in Table 1. The model is derived as described in **Section 3** and the speed/torque profile derivation is presented in **Section 2**. The thermal stress of the On-Demand drive inverter is compared for three different speed/torque profiles:

- Measured On-Demand drive machine torque and speed
- Estimated On-Demand drive torque based on simplified torque distribution strategy (**Approach A** in **Section 2**), and
- On-Demand drive torque obtained from torque mapping (**Approach B** in **Section 2**).

Parameter	Value	Unit
Peak torque $T_{pk}$	165	Nm
Peak power $P_{pk}$	80	kW
Max. motor speed $n_{max}$	13500	rpm
System voltage $V_{DC}$	400	V
Switching frequency $f_{sw}$	9 .. 11	kHz
Semiconductor type	Si IGBT	-

**Tab. 1:** On-Demand drive system parameters.

In Fig. 9, simulated junction temperature profiles are shown. The junction temperature profiles are simulated for torque profiles given in Fig. 5. Good match in junction temperatures can be observed between the measured drive cycle and the drive cycle derived using **Approach B** while the results for **Approach A** show deviations in the junction temperature compared to the measured drive cycle. For **Approach A**, the absolute mean error in the simulated junction temperature is  $3.4^\circ\text{C}$  and  $2.7^\circ\text{C}$  for **Approach B** when compared to the simulation results based on the measured speed/torque profile. The simulated temperature profiles are further used to estimate thermal stress of the inverter.

Thermal stress is derived by means of rain-flow counting implemented in MATLAB considering lifetime curves given by the manufacturer of the power module. The thermal stress profiles are depicted in Fig. 10. As can be observed, the stress profiles show very good match between the original torque

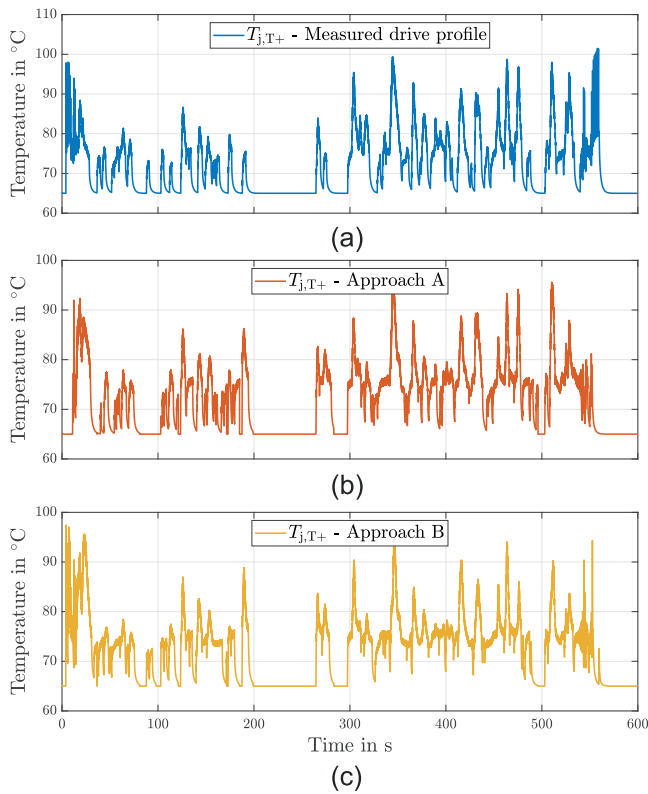


**Fig. 9:** Comparison of simulated junction temperature profiles for different drive usage approaches. (a) **Measured drive profile**, (b) synthetically derived drive profile based on **Approach A** and (c) derived drive profile based on **Approach B**.

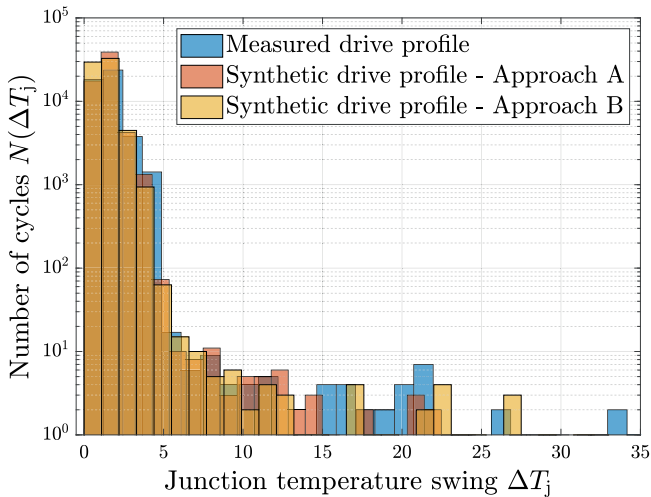


**Fig. 10:** Comparison of module thermal stress based on junction temperature swing for: **Measured drive profile**, synthetically derived drive profile based on **Approach A** and derived drive profile based on **Approach B**.

profile and the synthetic torque profile generated by means of torque mapping (**Approach B** from **Section 2**), especially for small junction temperature swings. However, for higher junction temperature

swings, the synthetic torque profile underestimates the effective thermal stress. This can be attributed to the averaging of the torque map generation approach.

## 5 Conclusion

This paper presents a procedure for estimating inverter thermal stresses in On-Demand drive systems based on a novel torque mapping approach and efficient electro-thermal simulation. The torque mapping approach shows good agreement with measurement data. Additionally, a detailed system model of the On-Demand drive is presented. The simulation model shows very good accuracy and low simulation time.

Modeling of inverter lifetime degradation based on different torque loading profiles is planned as a next step of the work.

## References

- [1] M. Yilmaz and P. T. Krein, "Review of battery charger topologies, charging power levels, and infrastructure for plug-in electric and hybrid vehicles," *IEEE Transactions on Power Electronics*, vol. 28, no. 5, pp. 2151–2169, 2013. DOI: 10.1109/TPEL.2012.2212917.
- [2] M. Tong, X. Liu, L. Sun, Z. Xu, M. Cheng, and Q. Zou, "Investigation of an integrated battery charger for EVs based on a dual-motor traction system," in *Proc. of the IEEE Transportation Electrification Conference and Expo, Asia-Pacific (ITEC 2022)*, 2022, pp. 1–5. DOI: 10.1109/ITECAsia-Pacific56316.2022.9942110.
- [3] A. Emadi, Y. J. Lee, and K. Rajashekara, "Power electronics and motor drives in electric, hybrid electric, and plug-in hybrid electric vehicles," *IEEE Transactions on Industrial Electronics*, vol. 55, no. 6, pp. 2237–2245, 2008. DOI: 10.1109/TIE.2008.922768.
- [4] J. A. P. Lopes, F. J. Soares, and P. M. R. Almeida, "Integration of electric vehicles in the electric power system," *Proceedings of the IEEE*, vol. 99, no. 1, pp. 168–183, 2011. DOI: 10.1109/JPROC.2010.2066250.
- [5] O. Nezamuddin, R. Bagwe, and E. Dos Santos, "A multi-motor architecture for electric vehicles," in *Proc. of the IEEE Transportation Electrification Conference and Expo (ITEC 2019)*, 2019, pp. 1–6. DOI: 10.1109/ITEC.2019.8790582.
- [6] V. Schwarzer and R. Ghorbani, "Drive cycle generation for design optimization of electric vehicles," *IEEE Transactions on Vehicular Technology*, vol. 62, no. 1, pp. 89–97, 2013. DOI: 10.1109/TVT.2012.2219889.

- [7] M. Shahjalal, T. Shams, S. B. Hossain, M. Rishad Ahmed, M. Ahsan, *et al.*, “Thermal analysis of Si-IGBT based power electronic modules in 50 kW traction inverter application,” *e-Prime - Advances in Electrical Engineering, Electronics and Energy*, vol. 3, p. 100 112, 2023. DOI: <https://doi.org/10.1016/j.prime.2023.100112>.
- [8] B. Zhao, N. Xu, H. Chen, K. Guo, and Y. Huang, “Design and experimental evaluations on energy-efficient control for 4WIMD-EVs considering tire slip energy,” *IEEE Transactions on Vehicular Technology*, vol. 69, no. 12, pp. 14 631–14 644, 2020. DOI: 10.1109/TVT.2020.3032377.
- [9] N. Mutoh, T. Kazama, and K. Takita, “Driving characteristics of an electric vehicle system with independently driven front and rear wheels,” *IEEE Transactions on Industrial Electronics*, vol. 53, no. 3, pp. 803–813, Jun. 2006. DOI: 10.1109/tie.2006.874271.
- [10] T. Kestler, V. Damec, and M.-M. Bakran, “Differences in dimensioning SiC MOSFETs and Si IGBTs for traction inverters,” in *Proc. of the 20th European Conference on Power Electronics and Applications (EPE 18 ECCE Europe)*, 2018, pp. 1–9.
- [11] K. Ma, U.-M. Choi, and F. Blaabjerg, “Prediction and validation of wear-out reliability metrics for power semiconductor devices with mission profiles in motor drive application,” *IEEE Transactions on Power Electronics*, vol. 33, no. 11, pp. 9843–9853, 2018. DOI: 10.1109/TPEL.2018.2798585.
- [12] M. Ouhab, Z. Khatir, A. Ibrahim, J.-P. Ousten, R. Mitova, and M.-X. Wang, “New analytical model for real-time junction temperature estimation of multichip power module used in a motor drive,” *IEEE Transactions on Power Electronics*, vol. 33, no. 6, pp. 5292–5301, 2018. DOI: 10.1109/TPEL.2017.2736534.
- [13] J. Ottosson, “Thermal modelling of power modules in a hybrid vehicle application,” Ph.D. dissertation, 2013.